Erschienen in: Nature methods ; 14 (2017), 10. - S. 995-1002
https://dx.doi.org/10.1038/nmeth.4399

Virtual reality for freely moving animals

John R Stowers[1,2], Maximilian Hofbauer[1–4], Renaud Bastien[5,6], Johannes Griessner[1], Peter Higgins[1], Sarfarazhussain Farooqui[3,4,7], Ruth M Fischer[3], Karin Nowikovsky[7], Wulf Haubensak[1], Iain D Couzin[5,6], Kristin Tessmar-Raible[3,4] & Andrew D Straw[1,8]

Standard animal behavior paradigms incompletely mimic nature and thus limit our understanding of behavior and brain function. Virtual reality (VR) can help, but it poses challenges. Typical VR systems require movement restrictions but disrupt sensorimotor experience, causing neuronal and behavioral alterations. We report the development of FreemoVR, a VR system for freely moving animals. We validate immersive VR for mice, flies, and zebrafish. FreemoVR allows instant, disruption-free environmental reconfigurations and interactions between real organisms and computer-controlled agents. Using the FreemoVR platform, we established a height-aversion assay in mice and studied visuomotor effects in *Drosophila* and zebrafish. Furthermore, by photorealistically mimicking zebrafish we discovered that effective social influence depends on a prospective leader balancing its internally preferred directional choice with social interaction. FreemoVR technology facilitates detailed investigations into neural function and behavior through the precise manipulation of sensorimotor feedback loops in unrestrained animals.

Sensory experience and motor output are, under natural conditions, inextricably linked in a perception–action cycle. Consequently, brains evolved to control behavior and process information dependent on movement and movement-related state[1–7]. Many physiological techniques to understand brain function require researchers to partially or fully immobilize animals; such techniques thereby disrupt sensory feedback, and this results in altered neuronal responses, even in central neurons. For example, the fraction of rodent hippocampal neurons showing sparse spatial response fields is strongly reduced when the restrained animal walks on a spherical treadmill, likely on account of the loss of vestibular feedback[8], whereas directional tuning of cells in the same region is largely unaffected[9]. Furthermore, our ability to mimic natural conditions in the laboratory are limited and strategies for doing so can be challenging to implement. Likewise, in order to unravel rules underlying social behavior, it is essential to manipulate interindividual interactions in reproducible ways with control over feedback and causality.

VR, defined as experimenter-controlled sensory–motor coupling, allows researchers to study behaviors and physiology for which feedback is important for the process under study. VR systems employed for animal research usually operate on restrained animals and provide a single modality of feedback such as visual[10–12] or tactile cues[13]. By restraining animals through such devices as a treadmill, VR allows precisely controlled stimulation[14] and brain activity imaging[2,15] or electrophysiological recording[10,16]. Thus, VR enables the study of brain responses connected to self-motion and to important aspects of natural conditions, such as photorealistic and perspective-correct visual sceneries. However, because systems for restrained animals usually restore feedback for a single modality, animals still lack normal coupling of the other senses. Even when VR has been used to test navigation in restrained animals by providing visual and auditory cues[17], coupling between visual and vestibular feedback remained unnatural.

Here we present a system that overcomes most of these limitations by immersing an unrestrained animal in a reactive, 3D world that is under computer control. We demonstrate the use of free-moving VR to unravel previously unnoticed behavioral differences, to perform experiments involving simulated teleportation and swarms to establish new decision-making paradigms, and to decipher rules that govern social interactions.

RESULTS

Implementation of FreemoVR

We built a VR system that simultaneously allows an animal to move freely and provides artificial visual feedback using the system's capability of simulating any desired visual scenery (**Fig. 1a–d**). This system, FreemoVR, maintains natural sensory–motor feedback for the mechanical senses while providing experimental control over the animal's visual experience. It uses animal tracking, precise spatial calibration of computer displays, and computer games technology to draw photorealistic and perspective-correct images from the animal's perspective as it walks, flies, or swims. We made use of computer vision to track animal position with low latency[18]. We built behavioral arenas whose walls or floors are computer

[1]Research Institute of Molecular Pathology, Vienna Biocenter, Vienna, Austria. [2]loopbio gmbh, Kritzendorf, Austria. [3]Max F. Perutz Laboratories, University of Vienna, Vienna, Austria. [4]Research Platform "Rhythms of Life," University of Vienna, Vienna, Austria. [5]Department of Collective Behaviour, Max Planck Institute for Ornithology, Konstanz, Germany. [6]Chair of Biodiversity and Collective Behaviour, Department of Biology, University of Konstanz, Konstanz, Germany. [7]Medizinische Universität Wien, Dept. for Internal Medicine I, Wien, Austria. [8]Institute of Biology I and Bernstein Center Freiburg, Faculty of Biology, Albert-Ludwigs-University Freiburg, Freiburg, Germany. Correspondence should be addressed to K.T.-R. (kristin.tessmar@mfpl.ac.at) or A.D.S. (straw@bio.uni-freiburg.de).

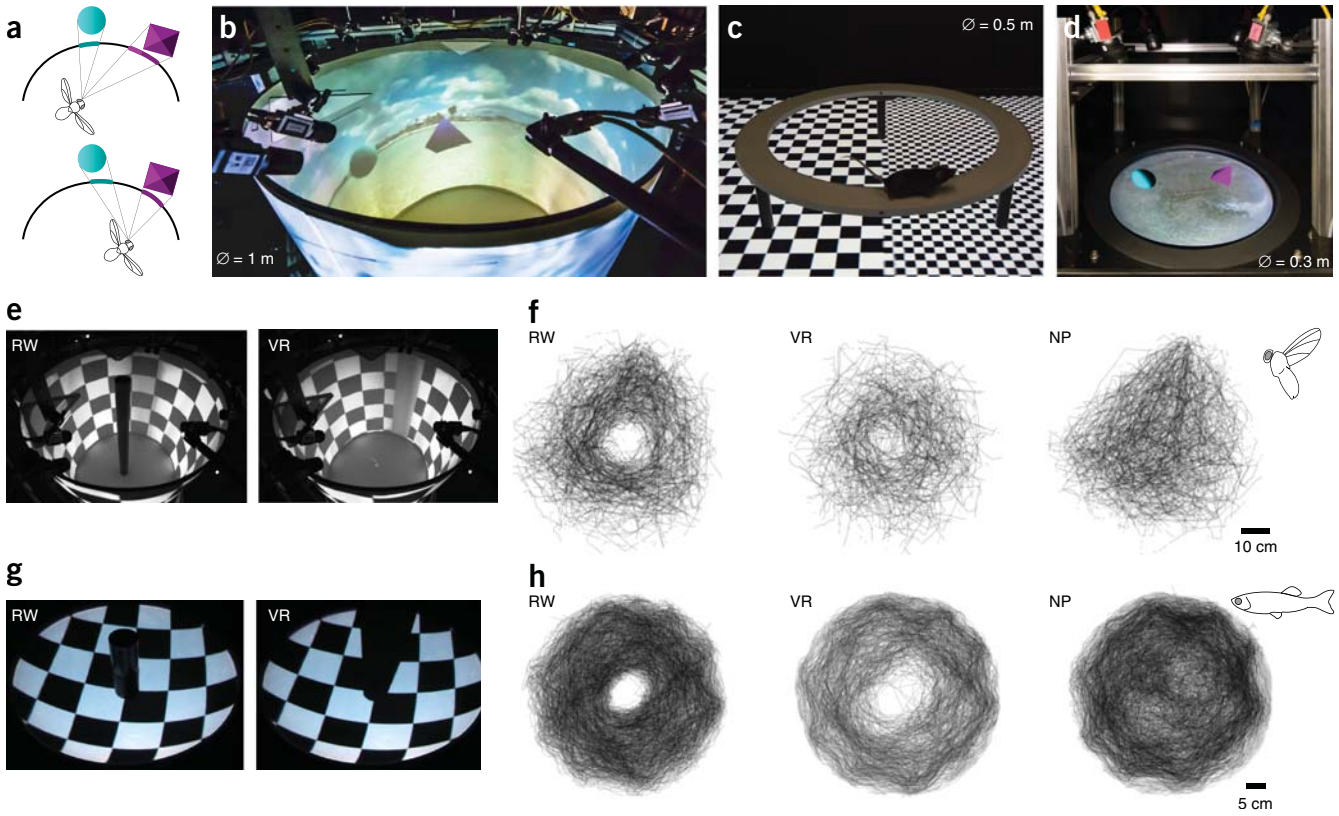

Figure 1 | FreemoVR virtual reality system for visual simulation. (**a**) Schematic illustrating perspective-correct projection of virtual objects onto a curved display surface. (**b**) The 'Flycave', a 1-m high, 1-m diameter cylindrical flight arena. Images are displayed on the walls of the cylinder using three projectors. (**c**) 'MouseVR', a VR apparatus for freely walking mice using a 1.9-m television for display. (**d**) 'FishVR', an apparatus in which zebrafish swim in 9-cm-deep water in a 32-cm diameter hemispherical bowl while a virtual environment is projected from beneath. The apparatus shows the same virtual scene as depicted in **b**. (**e**) Real-world (RW) and virtual reality (VR) post of 7.5-cm diameter at the center of a 1-m textured cylinder. (**f**) Top views of *Drosophila* trajectories over a 12-h trial in RW ($N = 25$ flies), VR ($N = 40$), and no-post (NP) ($N = 40$) conditions. (**g**) A 4-cm-diameter virtual post was simulated at the center of a 30-cm textured hemisphere. (**h**) Top views of zebrafish trajectories from 30-min trials in RW ($N = 11$), VR ($N = 13$), and no-post ('NP', $N = 13$) conditions.

displays including projection surfaces of any shape. Compared with other work[19–23], the innovations here include the ability to create sophisticated visual VR on arbitrarily shaped displays and the ability to do so for multiple species moving in 3D, including underwater. Flexibility in arena design and animal tracking allows the experimenter to choose tracking and display technologies best matched to the needs of a particular experiment (**Fig. 1**, **Supplementary Figs. 1** and **2**, **Supplementary Videos 1–4**, **Supplementary Software**, and https://www.strawlab.org/freemovr).

Validating behavioral responses to virtual objects and virtual environments

An ideal VR system would be able to mimic the sensory experience of real-world (RW) stimulation. If the VR system works reliably, animal behavior in response to a RW stimulus and the comparable VR stimulus should be similar. We therefore characterized flight trajectories of *Drosophila* in the presence of an upright gray post, placed at the center of an arena onto which a high-contrast checkerboard was projected (**Fig. 1e**). In response to both the RW object and the VR object, flies typically circled the post (**Fig. 1f**; **Supplementary Figs. 3** and **4**; and **Supplementary Videos 5** and **6**). In the no-post (NP) condition, identical to the RW and VR conditions except for the absence of the post, flies flew through the entire arena, including the center. Thus, flies behave as if they perceive the virtual and real objects similarly, which attests to the principle functionality of our system.

We performed similar experiments with juvenile zebrafish (46–56 d postfertilization (dpf)) in the presence of an upright black post at the center of a checkerboard-texture arena (**Fig. 1g**). To track the fish, we extended existing multicamera tracking software[18] with the new capability of correcting refraction from the air–water interface. Again, trajectories were consistent with animals perceiving the virtual object similarly to perceiving a real object (**Fig. 1h**, **Supplementary Video 7**).

These data indicate that our system generates naturalistic visual percepts of objects for freely moving animals.

Free-moving VR in a rodent innate aversion assay

Visual motion parallax from self-motion is important for rodents to estimate horizontal distance[24], and we wondered whether rodents estimate height similarly. We simultaneously asked this question and validated FreemoVR's effectiveness in mice with an assay measuring height aversion. The RW configuration (**Fig. 2a**) used a circular track placed above a shallow (20 cm) and a deep (40 cm) checkerboard surface. The VR configuration simulated these surfaces, and we also used a static (ST) configuration (**Fig. 2b**,**c** and **Supplementary Videos 8** and **9**). In RW and VR conditions, check size was 4 cm. Because of perspective, the shallow checks subtend larger visual angles than deep checks, and the ST condition showed checks of similar angular size but without correct motion parallax.

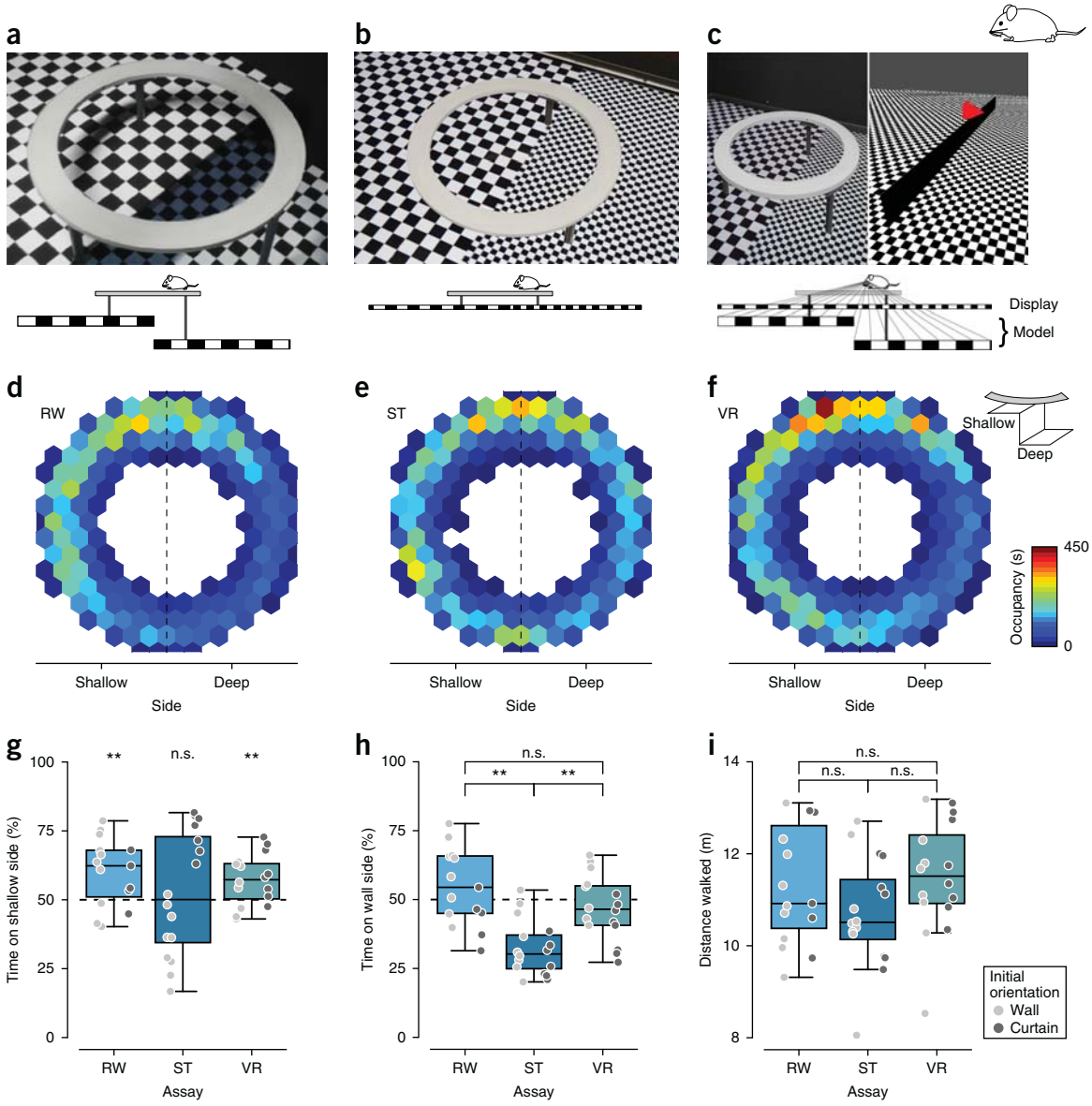

Figure 2 | Innate anxiety behavior to real and virtual elevated heights in mice. (**a**) Real world (RW) configuration of an elevated anxiety maze paradigm in which an '0' shaped platform is placed above checkerboards at different heights. (**b**) Stationary (ST) and (**c**) virtual reality (VR) configurations in which a television is placed under the '0' shaped platform. In VR, a perspective-correct simulation of the RW elevation maze is created using video-based head tracking, whereas in ST the displayed image does create motion parallax. (**d–f**) Top view of occupancy in the RW, ST, and VR configurations. (**g**) Time spent on the shallow side in each configuration. (**h**) Data replotted from **g** aligned to distant environmental cues to investigate the effect of the distal environmental cues. (**i**) Distance walked in each configuration. Values are mean of all animals. Error bars represent ±s.d. N = 15 mice for RW trials, N = 16 for VR, N = 16 for ST. n.s. = not significant, $P > 0.05$.

We found that mice spend more time above RW shallow surfaces but show no preference in ST conditions (**Fig. 2d,e**). In VR, mice spend more time above the simulated shallow surface (**Fig. 2f**), similar to their behavior in RW conditions. Statistically, the distribution of time spent per mouse on the shallow side was significantly different from that of a null hypothesis of 50% in both the RW and VR conditions, but not in the ST condition (**Fig. 2g**) (one sample t-test versus 50%, $P = 0.0072$, $N = 16$ mice (VR); $P = 0.0071$, $N = 15$ (RW); $P = 0.7152$, $N = 16$ (ST)). This shallow preference was overruled by static environmental cues, namely the preference for the side of the arena near a wall in the ST condition (**Fig. 2h** and **Supplementary Fig. 5a**) (one-way ANOVA $F(2,44) = 16$, $P < 0.0001$; Tukey's posthoc test; ST versus VR, $P = 0.0017$, $N = 16$ versus 16 mice; ST versus RW, $P < 0.0001$, $N = 16$ versus 15; VR versus RW, $P = 0.1456$, $N = 16$ versus 15; equal group variance, Bartlett test $P = 0.94$). Neither total locomotion nor head dipping was affected by these conditions (**Fig. 2i**; **Supplementary Figs. 5** and **6**) (one-way ANOVA $P = 0.18$; VR $N = 16$ mice, RW $N = 15$, ST $N = 16$, equal group variance, Bartlett test $P = 0.41$). Thus, FreemoVR can elicit height aversion in mice and, considering no such preference exists in static conditions, mouse aversion to height depends on parallax, not texture.

Altered action–perception in rigidly tethered *Drosophila*

We sought to determine the effect of a common experimental manipulation—head immobilization—in fly visuomotor control. In tethered flies, this manipulation maximizes precision of visual stimulation, enables electrophysiology, and has been important for studies of fly vision[5,25]. The few studies that investigated head

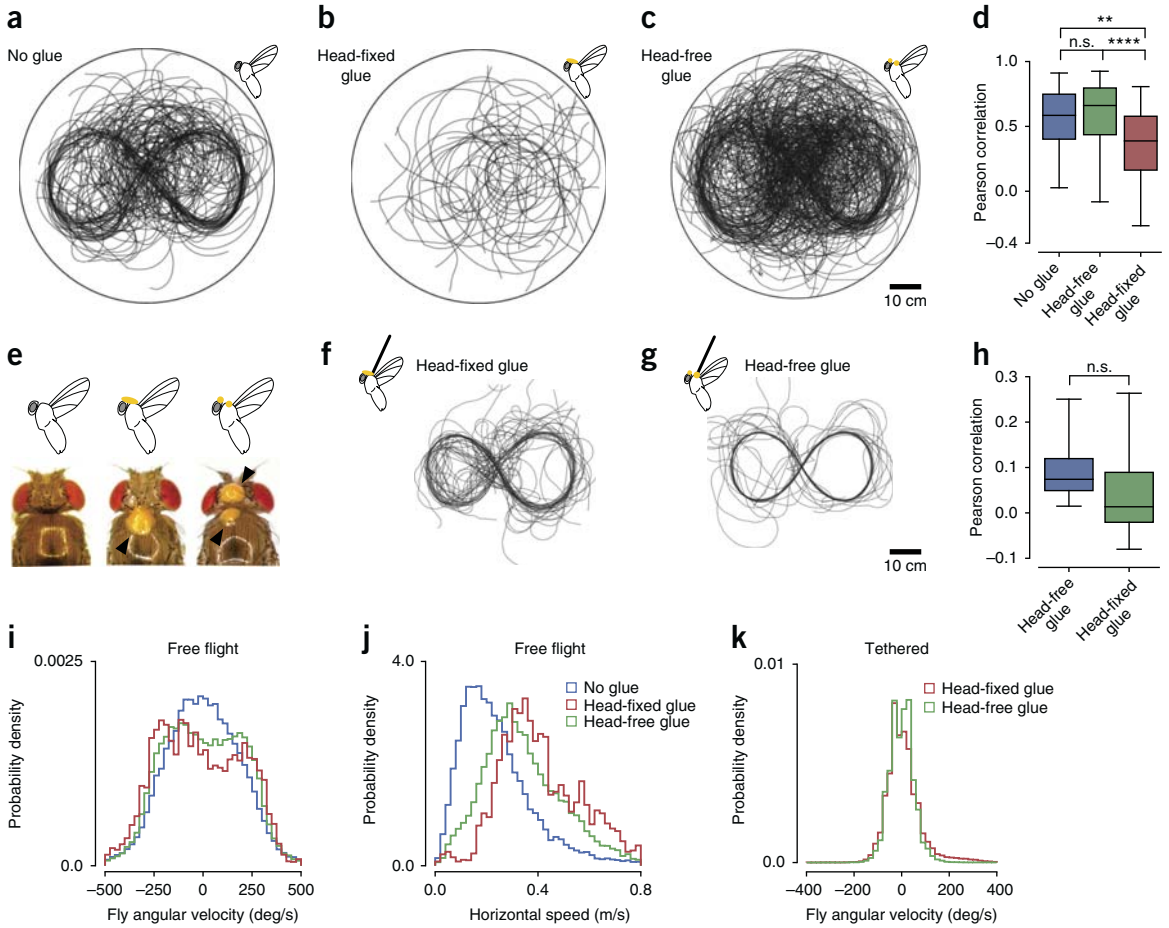

Figure 3 | Effect of head movement on *Drosophila* flight. (**a**–**c**) Top views of trajectories in which a freely flying fly was visually stimulated with VR-based panoramic image motion to keep it on an infinity symbol '∞' path. In **a**, no glue was applied (N = 36 flies), whereas in **b** the head was immobilized (N = 78). In **c**, glue was applied similarly to in **b**, but the droplets on head and thorax were not fused, and the head could thus move independently of the thorax (N = 39). (**d**) Correlation between angular velocity of the stimulus and fly trajectory at its maximum value. (**e**) Photographs of the glue application. (**f**,**g**) Top views of simulated tethered fly trajectories. In **f**, the heads were fixed as in **b** (N = 6). In **g**, the glue droplets on the head and thorax were not fused (N = 6). (**h**) Correlation between angular velocity of the stimulus and simulated fly trajectory at its maximum value. (**i**) Histogram of angular velocity for freely flying flies. (**j**) Histogram of horizontal speed for freely flying flies. (**k**) Histogram of simulated angular velocity for tethered flies. Histograms include data for all trials. Lagged correlations are the mean of trials from all individuals at latency 180 ms. Error bars for all plots represent ±s.d. For free flight experiments; head-fixed n trials = 34, head free n = 132, wild-type n = 55. For tethered experiments, head-fixed n trials = 11, head free n = 6. Box plots (**d**,**h**) indicate median, upper- and lower-quartile. Whiskers extend to 5 IQRs of the lower and upper quartile.

immobilization in tethered flight found confusing or minimal effects[26,27], whereas head movements are suggested to be important in free flight[28,29]. To date, no study has directly compared the effect of head immobilization in free versus tethered flight. Enabled by FreemoVR, we showed similar stimuli to tethered and freely flying flies and recorded behavioral performance.

For the free-flight experiments, we used the animals' own optomotor response to gather long behavioral trajectories in a limited spatial volume by coupling wide-field optic flow to the animals' position such that we could 'steer' the flies on an infinity-symbol (∞) shaped trajectory via visual rotation (**Fig. 3a**, **Supplementary Fig. 7**, and **Supplementary Video 10**). In the head-fixed group, the head was glued to the thorax, which prevented relative movement. In a control group, the glue droplet was prevented from fusing while hardening. These 'head-free glue' flies could still move their heads while having similar mechanical and sensory perturbations as head-fixed flies. Head-fixed flies flew relatively little (**Supplementary Table 1**) and, when they did, were unable to perform optomotor following in contrast to head-free glued and no-glue flies (**Fig. 3a**–**e**). Quantitatively, we found the correlation between visual stimulus and behavioral response significantly decreased in the head-fixed flies, while we measured no such difference in the head-free and wild-type flies with no glue (**Fig. 3d** and **Supplementary Fig. 8**) (Pearson correlation at lags 180 ms, Mann–Whitney test; no glue versus head fixed, P = 0.003, n trials = 55 versus 34; no glue versus head free, P = 0.20, n = 55 versus 132; head free versus head fixed, $P = 1.8 \times 10^{-5}$, n = 132 versus 34).

We performed corresponding experiments in rigidly tethered flies (**Fig. 3f**–**h**). Both head-fixed and head-free glued flies followed the optomotor stimulus, and we found no significant difference between groups (**Fig. 3h** and **Supplementary Fig. 8**) (Mann–Whitney test, head fixed versus head free, P = 0.20, n = 11 versus 6). Overall, the effect of head immobilization in free flight is unlikely caused by impaired mechanical maneuverability, because gluing caused little change in free-flight angular velocity statistics (**Fig. 3i**), and flight speed increased with glue application (**Fig. 3j**). In tethered flight,

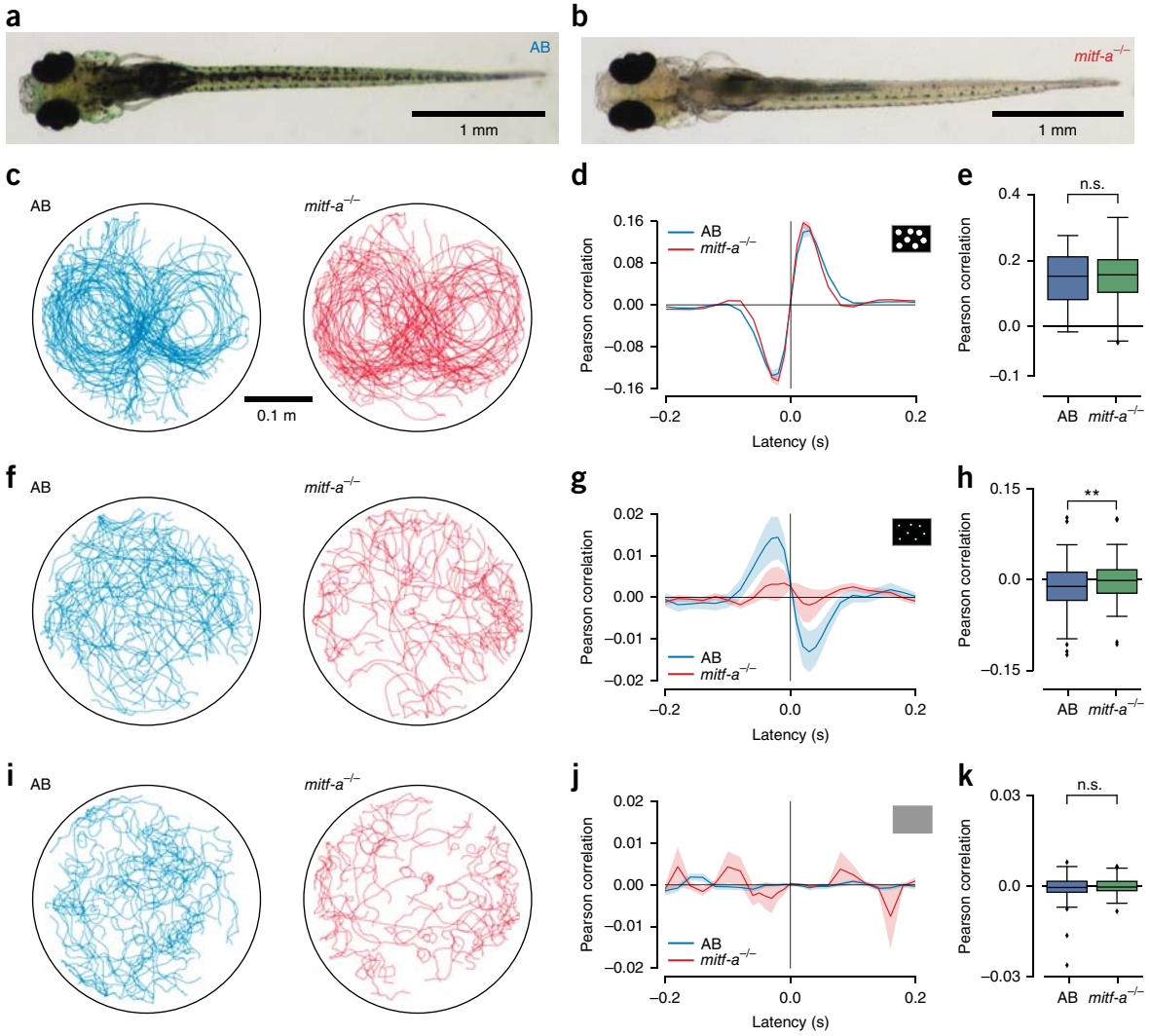

Figure 4 | Specific visuomotor deficit in *mitf-a*$^{-/-}$ zebrafish. (**a**) Photograph of wild-type (AB strain) and (**b**) *mitf*-a$^{-/-}$ mutant larvae (7 dpf). (**c**) Top views of trajectories of fish in infinity symbol '∞' assay in which a cloud of dots (angular size 3.1°) in 3D space was presented to wild-type and mutant fish. (**d**) Lagged Pearson correlation between lateral velocity of the visual motion in body coordinates and angular velocity of the swim trajectory for the two genotypes (mean ± 68% confidence interval, c.i.). (**e**) Maximal correlation in each condition (mean ± 68% c.i.). (**f**–**h**) As in **c**–**e** with smaller dots (angular size 1.3°). (**i**–**k**) As in **c**–**e** with a uniform zero-contrast background. Top views show a randomly selected 45-min subset of all data (**c**,**f**,**i**). *N* = 56 wild-type fish, *N* = 62 *mitf-a*$^{-/-}$ fish (6–9 dpf) tested. Box plots (**e**,**h**,**k**) indicate median, upper, and lower quartile. Whiskers extend to 1.5 IQRs of the lower and upper quartile.

head-fixed and head-free gluing resulted in little difference in the flies' angular velocity statistics (**Fig. 3k**). Our results indicate that tethered experiments, even without head fixation, cannot be used to study head movements for naturalistic flight control, because flight control is fundamentally altered by tethering.

A subtle visuomotor deficit in *mitf-a* mutant zebrafish

The zebrafish strain *nacre*, a *mitf-a* gene loss of function[30], has reduced pigmentation and is frequently used for whole-brain-activity imaging in combination with sensory–motor behavior[31]. Two previous investigations reported no behavioral differences between *nacre* and wild-type fish[32,33]. Given that behavioral differences exist even between wild-type strains[34,35], we wondered whether such differences might have gone unnoticed on account of the level of analysis or particular assays used. Automated VR system gives us the ability to test multiple visuomotor assay conditions by automatically and instantly reconfiguring the visual environment and experimental conditions with no physical disturbance.

We compared visuomotor behaviors of *nac*^{W2} mutant and wild-type AB larvae (**Fig. 4a**,**b**) using a modified infinity-symbol assay. We used a panoramic cloud of many circles, like a random-dot display, (**Supplementary Fig. 9** and **Supplementary Video 11**) to elicit compensatory movements by automatically adjusting dot 3D linear velocity. When tested with 3.1° dots, both *nac*^{W2} and wild-type fish robustly followed the target trajectory equally well (**Fig. 4c**), and the time-varying correlation between the lateral component of the input visual stimulus velocity and the output swim velocity showed no difference (**Fig. 4d**,**e**) (Pearson correlation at lags 20–30 ms Mann–Whitney test, $P = 0.52$, $n = 112$ trials for AB genotype; $n = 124$ trials for *mitf-a* genotype). With 1.3° dots, however, wild-type fish reversed the direction of their swim response, perhaps because of dot-size dependency[36] or spatial aliasing[37]. Mutant *mitf-a* fish showed near zero correlation (**Fig. 4f**–**h**), which was significantly different from that of wild-type fish (Mann–Whitney test, $P = 0.014$, $n = 112$ trials for AB genotype; $n = 124$ trials for *mitf-a* genotype). Control experiments with zero-contrast gray showed,

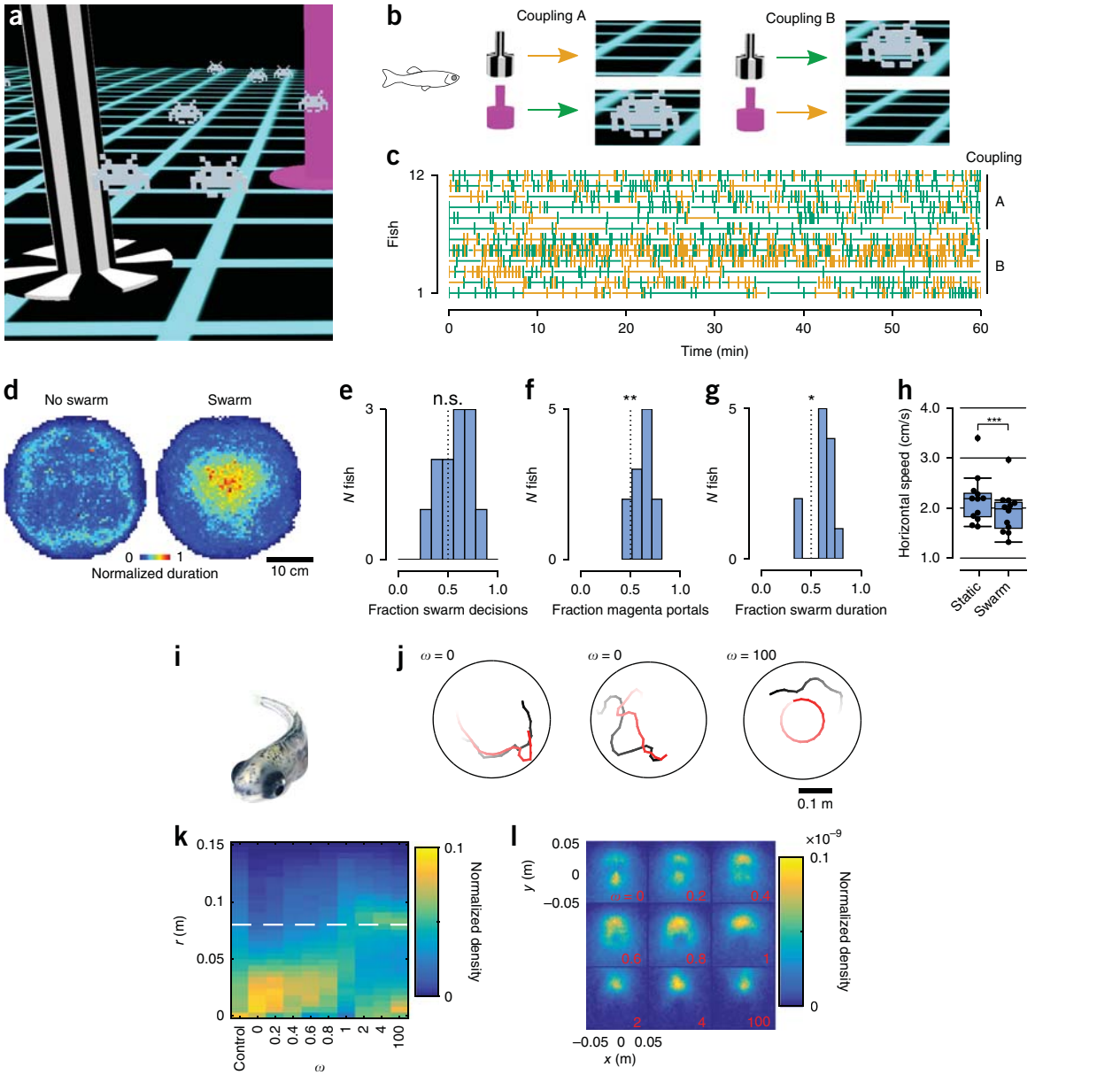

Figure 5 | Teleportation, swarms, and social feedback in virtual reality. (**a**) Zebrafish could trigger appearance of a moving swarm of space invaders by entering one portal and trigger disappearance by entering the other portal. (**b**) For each fish, coupling between portal appearance and swarm effect was constant, but different fish had different couplings. Upon entering a portal, the portals were rearranged to equalize distance required for subsequent portal entry. (**c**) Decisions (vertical marks) and current condition (horizontal line) of each fish. (**d**) Top view of occupancy. (**e**) Fraction of all decisions per fish coupled to swarm appearance. (**f**) Fraction of all portal entries per fish that were magenta. (**g**) Fraction of 60 min per fish in which the fish was in the presence of the swarm. (**h**) Mean horizontal speed per fish in each coupling condition. (**c**–**h**) $N = 12$ fish, AB strain. Box plots indicate median, upper, and lower quartile. Whiskers extend to 1.5 IQRs of the lower and upper quartile. (**i**) Image of virtual zebrafish, animated based on analysis of real zebrafish as shown in **Supplementary Figure 12**. (**j**) Example trajectories in which virtual fish (red color) is only influenced by the position of the real fish (black color) ($\omega = 0$), when it weights social influence and its internal preferred direction equally ($\omega = 1$), and when it strongly favors its internal preferred direction ($\omega = 100$). (**k**) Histogram of the real fish's distance from the periphery of the arena, r, as a function of the strength of the goal-oriented tendency, ω, of the virtual fish. Control condition shows real fish with no virtual fish present. The virtual fish's internal preferred trajectory was fixed at $r = 0.07$ m (dotted white) ($N = 16$ in all experiments with virtual fish, $N = 15$ in control experiments). (**l**) From the frame of reference of the real fish, the probability distribution of the location of the virtual fish at a given position ($N = 16$).

as expected, no correlation between stimulus and response and no significant difference (Mann–Whitney test, $P = 0.82$, $n = 112$ versus 124) between strains (**Fig. 4i**,**j**,**k**), and we found no obvious motor difference between strains (**Supplementary Fig. 10**). The behavioral alteration associated with the *mitf-a* strain is specific to the small point condition. This finding demonstrates the sensitivity and suitability of our VR system for discovering even relatively small derivations from wild-type behavior in freely moving animals.

Virtual teleportation to assess decision making in fish

To further demonstrate the novelty of experimental designs enabled by FreemoVR, we implemented a decision-making assay using virtual teleportation; when a fish entered a 'portal'—a special region with distinct visual appearance—an instantaneous simulated teleportation to a new environment occurred. We designed experiments in which a particular portal appearance was coupled with teleportation to a specific simulated environment (**Fig. 5a**–**c** and

Supplementary Fig. 11). We measured fish 'decisions', which are operationally defined as entering one of the two available portals. Two types of environmental settings were tested. In one of these the fish could choose between a checkerboard and a plant world (**Supplementary Fig. 11** and **Supplementary Video 12**), and in one scenario the fish could choose between the absence or presence of a virtual swarm (**Fig. 5a–h** and **Supplementary Video 13**). The swarm consisted of video game space invaders, each independently controlled but exhibiting flocking behavior, as the invaders were controlled by the boids algorithm[38]. Each simulated creature was programmed to respond to the real fish exactly as it responded to the other creatures. We found that fish were influenced by the swarm, as seen in the spatial occupancy distribution (**Fig. 5d**).

We tested if fish could associate a 'decision' (**Fig. 5b–h**) with the teleportation outcome. We kept the coupling constant in individual fish, but we tested the two possible couplings in different fish (**Fig. 5b**). We analyzed the results as a series of two alternative forced choice decisions and, in 1-h trials, found that fish decisions were not significantly biased for swarms or their absence (**Fig. 5e**, one-sample *t*-test difference from 0.5, $P = 0.34$). Fish preferred magenta portals (**Fig. 5f**, $P = 0.0025$) and spent more time in the swarm condition (**Fig. 5g**, $P = 0.014$), likely because they swam more slowly there (**Fig. 5h**, two-related-sample *t*-test, $P = 0.00029$). These teleportation experiments revealed scene-specific swimming speeds, occupancy differences, and preference for portal appearance; but they showed no learning.

Balancing internal preferred direction with social responsiveness is required for effective leadership in zebrafish

We addressed the question of how individuals reconcile personal and social information when making movement decisions, and we explored how the strength of feedback between a real and a virtual fish under computer control impacts leadership. Theoretical work suggests that an individual can exert influence while minimizing group splitting by balancing internal preferred travel direction with travel toward others[39].

We created a photorealistic virtual fish (**Fig. 5i**; **Supplementary Figs. 12** and **13**; and **Supplementary Video 14**) and adjusted its interactivity toward real fish. Zebrafish of this age (23 dpf), without social influence, predominantly swim around the arena periphery (**Fig. 5k**, control). We programmed our virtual fish to differ by preferring a trajectory around the arena center (0.07 m from the periphery; **Fig. 5k**, white dotted line). Thus, we created a conflict that allowed us to explore how social feedback—under computer control in the virtual fish—impacts movement.

We changed, via weighting factor ω[39–41], how strongly the virtual fish is influenced by its preferred central trajectory relative to swimming toward the real fish (see Online Methods). If $\omega = 0$, the virtual fish is exclusively influenced by the real fish. As ω increases, movement becomes more influenced by preferred direction, such that for $\omega = 1$, social and goal oriented are equal, and with $\omega > 1$, the virtual fish increasingly biases its motion toward its preferred direction.

When the virtual fish is influenced relatively weakly by its preferred trajectory ($\omega = 0$–0.2), the real fish dominates the direction of travel, and the virtual fish spends most time following it (**Fig. 5k**). In these conditions, both fish spend most time circling the perimeter of the arena (the real fish's preferred trajectory), and the real fish's distance from arena edge is near 0 m. This perimeter-circling behavior is similar to control conditions with no virtual fish (**Fig. 5k** and **Supplementary Fig. 14**). In this low-ω regime, probability histograms in body-centric coordinates for the real fish confirm that the virtual fish is most frequently immediately behind the real fish (**Fig. 5l**). As the virtual fish more equally weights the direction of the real fish into its own direction of travel ($\omega = 0.4$–4), the real fish is influenced by this social feedback, and thus its own position in the arena shifts away from edge following (**Fig. 5k**, $P < 10^{-5}$, Mann–Whitney U test comparing distance from edge for $\omega = 0$ to $\omega = 1$). This is associated with a change in the relative position; real fish now more frequently follow virtual fish (**Fig. 5l** and **Supplementary Fig. 15**). For still higher values of ω, when the virtual fish movement is dominated by its own preferred route ($\omega = 100$), the real and virtual fish often separate, with the real fish reverting back to edge following (**Fig. 5k**, $P < 10^{-5}$, Mann–Whitney U test comparing distance from edge for $\omega = 1$ to $\omega = 100$), and the relative positions are more variable, resulting in more uniform, and therefore less distinctly peaked, relative positions in the probability histograms of fish position (**Fig. 5l**). Thus, while reducing social feedback allows the virtual fish to exert a greater influence on the real fish, it also increases the risk of losing, and thus completely failing to lead, the real fish.

DISCUSSION

We demonstrate our FreemoVR system's ability to elicit naturalistic object responses in freely flying *Drosophila* and freely swimming zebrafish and anxiety-related behaviors in freely walking mice. Immersive, reactive VR has the potential to become an invaluable tool in the study of multimodal sensory integration, spatial cognition, social interactions, and collective behavior.

Despite its advantages, our system also has limitations. Because it renders visual stimuli in a perspective-correct manner for a single viewpoint, it is not directly suitable for the investigation of behaviors for which stereopsis is important or for simulating virtual worlds for multiple animals simultaneously. Here we have not tracked eye position or angular orientation, but these would be useful future additions. By using computer graphics cards and displays designed for humans, we enable the use of inexpensive and flexible hardware; but certain experiments, especially those on animals with visual requirements far different than our own, such as high temporal resolution or broad spectral and polarization sensitivity, will present further challenges.

When used together with technologies to measure neural activity in freely moving animals[42–45], VR for freely moving animals will advance investigation of brain function of high-level behaviors such as navigation. Additionally, the ability to programmatically control virtual agents will facilitate careful study of causality in collective behavior. Ultimately, this is important because it will allow researchers to study the mechanistic basis of behavior under conditions in which the brain evolved to operate.

ACKNOWLEDGMENTS

We thank M. Colombini, A. Fuhrmann, L. Fenk, E. Campione, S. Villalba, and the IMP/IMBA Workshop for help constructing FreemoVR hardware and software.

We thank M. Dickinson and T. Klausberger for helpful discussions, V. Böhm for help with experiments, and the MFPL fish facility for fish care. The manual mouse behavior annotation was performed by the Preclinical Phenotyping Facility at Vienna Biocenter Core Facilities. This work was supported by European Research Council (ERC) starting grants 281884 to A.D.S., 311701 to W.H., 337011 to K.T.-R.; Wiener Wissenschafts-, Forschungs- und Technologiefonds (WWTF) grant CS2011-029 to A.D.S.; FWF (http://www.fwf.ac.at/) research project grants P28970 to K.T.-R. and P29077 to K.N.; NSF grants PHY-0848755 to I.D.C., IOS-1355061 to I.D.C., EAGER-IOS-1251585 to I.D.C.; ONR grants N00014-09-1-1074 to I.D.C., N00014-14-1-0635 to I.D.C; ARO grants W911NG-11-1-0385 to I.D.C., W911NF-14-1-0431 to I.D.C. A.D.S and W.H. were further supported by the IMP, Boehringer Ingelheim and the Austrian Research Promotion Agency (FFG). K.T.-R. is supported by grants from the University of Vienna (research platform "Rhythms of Life"). IDC acknowledges further support from the "Struktur- und Innovationsfonds für die Forschung (SI-BW)" of the State of Baden-Württemberg and from the Max Planck Society. I.D.C. and R.B. gratefully acknowledge fish care and technical support from C. Bauer, J. Weglarski, A. Bruttel, and G. Mazué.

AUTHOR CONTRIBUTIONS

A.D.S., K.T.-R., W.H., and I.D.C. conceived the projects. J.R.S., M.H., R.M.F., R.B., and A.D.S. developed the hardware and software and built the apparatus. J.R.S., M.H., R.B., J.G., P.H., S.F., and A.D.S. performed experiments. J.R.S., M.H., R.B., J.G., S.F., W.H., I.D.C., K.T.-R. and A.D.S. performed data analyses. A.D.S., K.T.-R., I.D.C., J.R.S., M.H., and J.G. wrote the manuscript. A.D.S., K.T.-R., W.H., I.D.C., and K.N. funded the work. J.R.S. and M.H. contributed equally to this work. J.G., P.H., and S.F. contributed equally to this work.

1. Aghajan, Z.M. *et al.* Impaired spatial selectivity and intact phase precession in two-dimensional virtual reality. *Nat. Neurosci.* **18**, 121–128 (2015).
2. Chiappe, M.E., Seelig, J.D., Reiser, M.B. & Jayaraman, V. Walking modulates speed sensitivity in *Drosophila* motion vision. *Curr. Biol.* **20**, 1470–1475 (2010).
3. von Holst, E. & Mittelstaedt, H. Das Reafferenzprinzip - Wechselwirkungen zwischen Zentralnervensystem und Peripherie. *Naturwissenschaften* **37**, 464–476 (1950).
4. Jung, S.N., Borst, A. & Haag, J. Flight activity alters velocity tuning of fly motion-sensitive neurons. *J. Neurosci.* **31**, 9231–9237 (2011).
5. Kim, A.J., Fitzgerald, J.K. & Maimon, G. Cellular evidence for efference copy in *Drosophila* visuomotor processing. *Nat. Neurosci.* **18**, 1247–1255 (2015).
6. Leinweber, M. *et al.* Two-photon calcium imaging in mice navigating a virtual reality environment. *J. Vis. Exp.* **20**, e50885 (2014).
7. Sperry, R.W. Neural basis of the spontaneous optokinetic response produced by visual inversion. *J. Comp. Physiol. Psychol.* **43**, 482–489 (1950).
8. Ravassard, P. *et al.* Multisensory control of hippocampal spatiotemporal selectivity. *Science* **340**, 1342–1346 (2013).
9. Acharya, L., Aghajan, Z.M., Vuong, C., Moore, J.J. & Mehta, M.R. Causal influence of visual cues on hippocampal directional selectivity. *Cell* **164**, 197–207 (2016).
10. Harvey, C.D., Collman, F., Dombeck, D.A. & Tank, D.W. Intracellular dynamics of hippocampal place cells during virtual navigation. *Nature* **461**, 941–946 (2009).
11. Schmidt-Hieber, C. & Häusser, M. Cellular mechanisms of spatial navigation in the medial entorhinal cortex. *Nat. Neurosci.* **16**, 325–331 (2013).
12. Aronov, D. & Tank, D.W. Engagement of neural circuits underlying 2D spatial navigation in a rodent virtual reality system. *Neuron* **84**, 442–456 (2014).
13. Sofroniew, N.J., Cohen, J.D., Lee, A.K. & Svoboda, K. Natural whisker-guided behavior by head-fixed mice in tactile virtual reality. *J. Neurosci.* **34**, 9537–9550 (2014).
14. Hölscher, C., Schnee, A., Dahmen, H., Setia, L. & Mallot, H.A. Rats are able to navigate in virtual environments. *J. Exp. Biol.* **208**, 561–569 (2005).
15. Dombeck, D.A., Harvey, C.D., Tian, L., Looger, L.L. & Tank, D.W. Functional imaging of hippocampal place cells at cellular resolution during virtual navigation. *Nat. Neurosci.* **13**, 1433–1440 (2010).
16. Maimon, G., Straw, A.D. & Dickinson, M.H. Active flight increases the gain of visual motion processing in *Drosophila*. *Nat. Neurosci.* **13**, 393–399 (2010).
17. Cushman, J.D. *et al.* Multisensory control of multimodal behavior: do the legs know what the tongue is doing? *PLoS One* **8**, e80465 (2013).
18. Straw, A.D., Branson, K., Neumann, T.R. & Dickinson, M.H. Multi-camera real-time three-dimensional tracking of multiple flying animals. *J. R. Soc. Interface* **8**, 395–409 (2011).
19. Fry, S.N., Rohrseitz, N., Straw, A.D. & Dickinson, M.H. Visual control of flight speed in *Drosophila melanogaster*. *J. Exp. Biol.* **212**, 1120–1130 (2009).
20. Schuster, S., Strauss, R. & Götz, K.G. Virtual-reality techniques resolve the visual cues used by fruit flies to evaluate object distances. *Curr. Biol.* **12**, 1591–1594 (2002).
21. Straw, A.D., Lee, S. & Dickinson, M.H. Visual control of altitude in flying *Drosophila*. *Curr. Biol.* **20**, 1550–1556 (2010).
22. Stowers, J.R. *et al.* Reverse engineering animal vision with virtual reality and genetics. *Computer* **47**, 38–45 (2014).
23. Del Grosso, N., Graboski, J., Chen, W., Blanco-Hernández, E. & Sirota, A. Virtual reality system for freely-moving rodents. Preprint at http://www.biorxiv.org/content/early/2017/07/10/161232 (2017).
24. Ellard, C.G., Goodale, M.A. & Timney, B. Distance estimation in the Mongolian gerbil: the role of dynamic depth cues. *Behav. Brain Res.* **14**, 29–39 (1984).
25. Poggio, T. & Reichardt, W. A theory of the pattern induced flight orientation of the fly Musca domestica. *Kybernetik* **12**, 185–203 (1973).
26. Duistermars, B.J., Care, R.A. & Frye, M.A. Binocular interactions underlying the classic optomotor responses of flying flies. *Front. Behav. Neurosci.* **6**, 6 (2012).
27. Reiser, M.B. & Dickinson, M.H. Visual motion speed determines a behavioral switch from forward flight to expansion avoidance in *Drosophila*. *J. Exp. Biol.* **216**, 719–732 (2013).
28. Kress, D. & Egelhaaf, M. Head and body stabilization in blowflies walking on differently structured substrates. *J. Exp. Biol.* **215**, 1523–1532 (2012).
29. Schilstra, C. & Hateren, J.H. Blowfly flight and optic flow. I. Thorax kinematics and flight dynamics. *J. Exp. Biol.* **202**, 1481–1490 (1999).
30. Lister, J.A., Robertson, C.P., Lepage, T., Johnson, S.L. & Raible, D.W. *nacre* encodes a zebrafish microphthalmia-related protein that regulates neural-crest-derived pigment cell fate. *Development* **126**, 3757–3767 (1999).
31. Ahrens, M.B. *et al.* Brain-wide neuronal dynamics during motor adaptation in zebrafish. *Nature* **485**, 471–477 (2012).
32. O'Malley, D.M. *et al.* Optical physiology and locomotor behaviors of wild-type and *nacre* zebrafish. *Methods Cell Biol.* **76**, 261–284 (2004).
33. Antinucci, P. & Hindges, R. A crystal-clear zebrafish for *in vivo* imaging. *Sci. Rep.* **6**, 29490 (2016).
34. Lange, M. *et al.* Inter-individual and inter-strain variations in zebrafish locomotor ontogeny. *PLoS One* **8**, e70172 (2013).
35. Liu, Y. *et al.* Statistical analysis of zebrafish locomotor response. *PLoS One* **10**, e0139521 (2015).
36. Barker, A.J. & Baier, H. Sensorimotor decision making in the zebrafish tectum. *Curr. Biol.* **25**, 2804–2814 (2015).
37. Thibos, L.N., Still, D.L. & Bradley, A. Characterization of spatial aliasing and contrast sensitivity in peripheral vision. *Vision Res.* **36**, 249–258 (1996).
38. Reynolds, C.W. Flocks, herds and schools: a distributed behavioral model. *Computer Graphics* **21**, 25–34 (1987).
39. Couzin, I.D., Krause, J., Franks, N.R. & Levin, S.A. Effective leadership and decision-making in animal groups on the move. *Nature* **433**, 513–516 (2005).
40. Couzin, I.D. *et al.* Uninformed individuals promote democratic consensus in animal groups. *Science* **334**, 1578–1580 (2011).
41. Ioannou, C.C., Guttal, V. & Couzin, I.D. Predatory fish select for coordinated collective motion in virtual prey. *Science* **337**, 1212–1215 (2012).
42. Naumann, E.A., Kampff, A.R., Prober, D.A., Schier, A.F. & Engert, F. Monitoring neural activity with bioluminescence during natural behavior. *Nat. Neurosci.* **13**, 513–520 (2010).
43. Randlett, O. *et al.* Whole-brain activity mapping onto a zebrafish brain atlas. *Nat. Methods* **12**, 1039–1046 (2015).
44. Szuts, T.A. *et al.* A wireless multi-channel neural amplifier for freely moving animals. *Nat. Neurosci.* **14**, 263–269 (2011).
45. Ziv, Y. *et al.* Long-term dynamics of CA1 hippocampal place codes. *Nat. Neurosci.* **16**, 264–266 (2013).

ONLINE METHODS

Implementation of the FreemoVR engine. The FreemoVR Engine is software written in C++ and uses the OpenSceneGraph library for rendering. Different virtual worlds or other experimental paradigms can be programmed as plugins, and a general purpose plugin for rendering complete 3D scenes (OSG format files) is included. Other plugins for custom rendering can be developed while using the FreemoVR projector calibrations and rendering infrastructure. Provided plugins include those for drawing 3D random dot patterns. OSG format 3D scenes can be designed using modeling software such as Blender. The FreemoVR Engine runs as part of a larger FreemoVR System built on the robot operating system (ROS). Experiments and experimental logic are written in Python and communicate with other parts of the system using the ROS interprocess communication and multiprocess launching and parameter setting framework. The FreemoVR Engine itself does not depend on specific tracking software; it works with any tracking implementation that provides 3D position. The tracking implementations used within the FreemoVR System for the experiments presented are discussed below.

High-level control of VR experiments is implemented in a separate process (the 'experimental node') from the FreemoVR Engine and the tracking program. This experimental node enforces the starting and stopping criteria for every trial over the duration of the experiment, changes between different stimulus conditions, and alters the real world in real time if required (such as in the case of path-following trials).

All experiments presented in the manuscript make use of stimuli whose precise nature depends on the translational (x,y,z) position of the animal's eyes but does not attempt to alter closed loop visual feedback in the rotational axes (yaw, pitch, roll) other than to add constant rotational bias. (In **Fig. 3**, rotational bias was added by rotating the stimulus in world coordinates without attempting to compensate for the animal's orientation.) In other words, we did not attempt to alter the visuomotor feedback loop with respect to rotation, but only with translation.

The FreemoVR software is available from https://strawlab.org/freemovr and is included in **Supplementary Software**, as is the tracking software.

Measuring latency and its behavioral effects. Given the physical coupling between animal motion and sensory feedback under natural conditions, we wondered how the latency of our system—the total duration between movement of the subject and a compensatory reaction by the display—might affect these results. For the different VR systems we implemented, we made latency measurements and found values between 60 and 75 ms (**Supplementary Fig. 3c**), with more than half the total latency caused by rendering on the graphics card and display on the monitor or projector. To address the question of how latency affects our results, we measured behavioral performance, the turning rate of a fly turning away from a rapidly nearing object, as we artificially varied latency. As we approached the smallest possible latencies of our system (0 ms added latency, 60 ms total latency), turn rate asymptotically approached ~50°/s, and turns in response to the VR object were not measurably different than turns in response to the RW object (**Supplementary Figs. 3** and **4**), (Mann–Whitney test, $P = 0.82$, difference between mean of all turns toward post, $n = 109$ versus 99 trials, group variance not different, Baretts test $P = 0.66$), while longer artificial latencies reduced post-avoidance turning.

Animal handling. All animal work was conducted according to Austrian, German and European laws and guidelines for animal research.

Zebrafish. All fish used in **Figures 1**, **4**, and **5a**–**h** were bred and raised by the fish facility of the Max F. Perutz Laboratories Vienna (BMWFW-66.006/0012-WF/II/3b/2014 and BMWFW-66.006/0003-WF/V/3b/2016). Zebrafish (*Danio rerio*) strains AB and *mitf*-a were kept in a constant recirculating system at 28 °C on a 16 h light/8 h dark cycle. Collected embryos were kept at 28 °C until hatched. Water was stored in the experimental room to have the same temperature as the experimental apparatus. All fish were moved to the experimental room at least 12 h before testing. Powdered food was available constantly in the holding containers for this period. The water in the experimental apparatus was changed each day before the first experiment except if protocol demanded differently. All fish were tested individually; they were naive and picked at random from the tanks they were raised in. We did not perform size selection for the experiments in **Figures 1** and **4**. For experiments in **Figure 5a**–**h**, relatively large fish were selected.

All fish used in **Figure 5i**–**l** were bred and raised by the animal care staff of the Department of Collective Behavior (University of Konstanz/Max Planck Institute). 16 h before conducting experiments, water from the fish facility was taken to the experimental room in order to ensure that water conditions in the VR arenas was the same as in the holding facility. The experimental room was kept at 28 °C. All fish were moved to the experimental room at least 12 h before testing and kept on a 16:8 day:night light regime, as in the fish facility. The water in the experimental apparatus was changed each day before the first experiment. All fish were tested individually; they were naive and picked at random from the tanks they were raised in (according to the animal ethics permit approved by Regierungspräsidium Freiburg, G-16/158).

Drosophila. All experiments were performed on wild-type CS strain *Drosophila melanogaster*. Flies were raised at 22 °C on a 12-h light, 12-h dark cycle.

Mice. Mice were C57BL/6J males purchased from Charles River Laboratories (Sulzfeld, Germany) and 5–6 months old at time of testing. Animals were group housed at 21 °C, and food and water were provided *ad libitum* in a 14 h light and 10 h dark cycle (day starting at 6:00 a.m.), not adjusted for daylight savings time during the summer. All tests were performed during the light period. All mouse experiments were performed in accordance with institutional guidelines and were approved by the respective Austrian (BGBl nr. 501/1988, idF BGBl I no. 162/2005) and European (Directive 86/609/EEC of 24 November 1986, European Community) authorities and covered by the license MA58/002220/2011/9.

Behavioral setups. A parts list for all setups can be found in **Supplementary Tables 2**–**4**.

FishVR (zebrafish). The bowl was constructed from acrylic by Immersive Display Group, London, UK and is a subsection of a sphere with a diameter of 40.6 cm. The bowl is filled with 4.5 l of water resulting in a depth of 9.1 cm and a diameter of 33.8 cm. Infrared light for tracking of a wavelength of 850 nm is provided

from underneath the bowl. The projection illuminates the entire surface of the bowl under water level. We used an LED DLP projector (Optoma ML500) with vsync enabled on the graphics card. The water surface is protected against dust and airflow with a hood that also covers the cameras.

A computer (Intel, Core i7, nVidia GeForce GTX 960) does all tracking and VR computation. Four cameras (Basler acA640) mounted outside the water acquire images at 100 fps. Fish position is tracked at 100 fps. A correction for the refraction of light through the water surface is made in real time (see "Animal tracking").

*FlyCave (*Drosophila*).* The flight arena is a 1 m diameter, 1 m high translucent cylinder constructed from projection material (Gerriets International Opera Creamy White Front/Back) bonded to lampshade backing PVC (generic brand, translucent, 0.3 mm thick) for structural support. The cylinder is freestanding and is capped on the top and bottom by sheets of transparent Perspex. There are two mesh-covered openings in the top cover of the arena to allow cool air to circulate. The room in which the arena stands is temperature controlled at 20.5 °C. Ten cameras (Basler acA640) are distributed around the top of the cylinder, and their field of view and focus depth are adjusted to cover the whole arena.

The VR is projected onto the outside of the cylinder using three projectors (Mitsubishi WD-385U-EST) projectors operating at 1,024 × 768 pixel resolution and 120 Hz refresh rate.

One computer (Intel, Core i5, nVidia GeForce GTX 670 rev a1) does 3D computations and VR projection; and two further computers (Intel, Core i5) track 2D fly positions at 100 fps. Flies were tracked with 850 nm IR light.

MouseVR (mouse). A 1.9 m (75″, Sony KDL-75W855CBAEP) was used to display the VR. A single camera (Basler acA640) was mounted centrally above the television. Mouse head position was tracked in 2D under 850 nm IR light using custom software (**Supplementary Software**). 3D position was estimated by assuming the mouse had remained at a fixed altitude. A single computer (Intel, Core i7, nVidia GTX 670) did all tracking and VR computation in real time.

The elevated circular platform measures 0.5 m (external diameter), and 0.0396 m (internal diameter), giving the ring platform a width of 52 mm. The ring was constructed from light-gray PVC. The ring is 10 mm thick and has a 2 mm high ridge on the inner and outer sides to make it harder for mice to slip off. In VR trials the ring was placed 13.4 cm above the television surface. The ring sits atop three 2 cm diameter legs made from dark PVC and placed at 120° from one another.

Light measurements were recorded (PCE-174 Lux Meter) for VR and RW trials. Looking down, the illumination was 100 l× and 35–60 l×, respectively. Looking up, they were 2 l× and 250–370 l×, respectively.

Experimental methods. *Statistical reporting.* Number of animals is reported with *N*, number of trials with *n*.

Zebrafish post experiments. Zebrafish of the AB strain with an age between 46 and 56 dpf were used (**Fig. 1**). They were picked at random from two breeding tanks. Zebrafish varied in size from 7–15 mm. Testing blind to the condition was not possible, but all evaluation was done by automated computer programs, and thus blinding was not necessary for analysis. In total we tested 24 fish; 13 for VR post and control condition and 11 for the real post condition. One fish was in the assay at each time. A new fish was used for each experiment. NP condition was followed by VR condition; RW experiments were performed separately. Conditions were presented for 30 min. NP/VR experiments took 1 h; RW experiments took 30 min. When changing experiments from NP/VR to RW, or from RW to NP/VR, the water was changed. Experiments were performed at room temperature, 22–25 °C.

The RW post was 15 cm high and 4 cm in diameter and milled from black Delrin. The VR post was modeled to the same size, and it was placed inside a checkerboard-textured sphere of the same size as the physical bowl. The VR model was generated with blender (2.74), exported to OpenSceneGraph formal (osg), and loaded directly by FreemoVR. Experimental data files are included in **Supplementary Software**. In VR trials, the VR post and bowl were present. In RW and NP trials, the VR post was made invisible, but the textured bowl remained.

Sample size was not predetermined. Experiments were run until top views of the trajectories covered the arena densely.

Starting and stopping criteria. Trials were started when a fish was detected in the bowl and underwater. Trials were stopped when the fish was not detected for 0.5 s, when any position estimate for the fish was outside of the bowl or 2 cm above the water level, or when the stimulus condition changed.

Zebrafish path-following experiments. Zebrafish larvae of the wild type AB strain and *nacre* mutant were tested 6–9 dpf (**Fig. 4**). We chose AB because the nac^{W2} mutation was generated in this wild-type background[31]. Larvae were tested for 45 min each between 10:00 and 19:00. Sample size was determined by the number of fish resulting from a laboratory-typical breeding cycle. In total 62 fish from the *mitf*-$a^{-/-}$ strain were tested, as were 56 age-matched larvae from wild-type AB strain reared under identical conditions. This sample size resulted after excluding experiments with technical (projector malfunction) or environmental disturbances (construction-related vibration and noise). Blind testing with regard to strain or experimental condition was not possible, but all evaluation was done by automated computer programs, and thus blinding was not necessary. If possible, tests were shuffled between the two genotypes. Experiments were performed at room temperature, 22–25 °C.

A cloud of 3D dots was designed to elicit the optomotor response and thus path following. The stimulus was generated by the agglomeration of identical white dots randomly positioned in a 3D volume of 1 × 1 × 1 m volume. All dots moved with identical velocity. The origin of the dot cloud was fixed to the position of the fish. The velocity of the dots, $\boldsymbol{V} = (V_x, V_y, V_z)^{\mathrm{T}}$, was calculated by a closed loop position proportional control law which tries to bring the active fish position to a target point on the path. More exactly,

$$V_x = (X_{\text{target}} - X_{\text{fly}})K_{\text{horizontal}}$$
$$V_y = (Y_{\text{target}} - Y_{\text{fly}})K_{\text{horizontal}}$$
$$V_z = 0$$

where $K_{\text{horizontal}}$ is the feedback gain for path following, and K_{vertical} is the feedback gain for altitude control. When the active fish position was within 0.1 m of the target position, the target position was advanced to the next point along the path.

Three experimental conditions were tested; 'large dots', 'small dots', and 'gray'. The 'large dot' angular size was 3.1°. The 'small dot' condition angular size was 1.3°. In the 'gray' condition,

a static texture less gray color was shown. Conditions were randomly ordered and then alternated sequentially every 5 min.

Sample size was determined by the number of fish we could test in a single week of the correct genotypes for a single replicate. Three replicates were performed using three separate egg batches.

Starting and stopping criteria. Trials were started when a fish was in a cubic volume $-0.15\ \text{m} < x < 0.15\ \text{m}$, $-0.15\ \text{m} < y < 0.15\ \text{m}$, $-0.10\ \text{m} < z < 0.01\ \text{m}$. Trials ended when the active fish average speed over 1 s was less than 1 mm/s, when the active fish performing the trial had not been detected for 0.5 s, or when the stimulus condition changed.

Zebrafish virtual teleportation and swarm experiments. Zebrafish of the AB strain with an age between 24 and 30 dpf were used (**Fig. 5a**–**h**). Testing blind to experiment condition was not possible, but all evaluation was done by automated computer programs, and thus blinding was not necessary. In total we tested 24 fish; 12 for virtual teleportation and 12 for swam experiments. One fish was in the assay at each time. A new fish was used for each experiment. Virtual teleportation experiments lasted 30 min, and the swarm experiment trials were 1 h. Experiments were performed at 28 °C.

Sample size was determined by the time available to perform experiments combined with fish availability.

Zebrafish social feedback experiments. We used 31 juvenile wild-type zebrafish (23 dpf, body length 9.5 mm ± 0.5 mm) picked at random from one breeding tank (**Fig. 5i**–**l**). Each individual was tested once for 90 min between 10:00 and 19:00. 16 fish were tested with VR stimuli and 15 with no VR stimuli (control condition). Sample size was determined by the time available to perform experiments combined with fish availability.

A virtual fish (VF), 3D mesh and texture mapping was generated by ENGELS Visualisierungen from multiple images of a zebrafish larvae (9.5 mm). The tailbeat movement of the VF was animated with blender based on median-line-tracking data from video extracted using the software KymoRod[46]. A linear straight chain of 32 bones was applied to the mesh, and this was animated, based on the extracted tracking data, with an oscillating wave propagating from the head to the tail (**Supplementary Fig. 12**).

The movement of the zebrafish larvae is described as burst and glide motion. A first phase of propulsion is followed by a glide movement that is damped by the friction with water. A new burst and glide movement was generated each $t_{tb} = 0.5$ s. During this movement, the linear velocity was described by an exponential function

$$V_r = V_0 e^{-t/t_c}$$

with $t_c = 0.25$ s and $V_0 = 0.14\ \text{ms}^{-1}$. The direction of the VF, $\mathbf{d}_{VF}$,was updated at the beginning of each burst and glide event and determined in accordance with the model previously described [39,40]. Following this model, avoidance of collisions is the highest priority of the VF. We define a repulsion zone of size $l_r = 2$ cm. When the distance between the real fish (RF) and the VF, $l_{vf} = \sqrt{(x_{RF} - x_{VF})^2 + (y_{RF} - y_{VF})^2}$, is smaller than the distance of repulsion, l_r,the VF turns away from the RF. The direction of the VF is then given by

$$\mathbf{d}_{VF} = -\frac{(x_{RF} - x_{VF})\mathbf{e}_x + (y_{RF} - y_{VF})\mathbf{e}_y}{l_{vf}}$$

If the RF is outside of the repulsion zone, the VF balance the influence of its preferred direction, $\boldsymbol{g}$, and their attraction to the RF

$$\mathbf{d}_{VF} = -\frac{(x_{RF} - x_{VF})\mathbf{e}_x + (y_{RF} - y_{VF})\mathbf{e}_y}{l_{vf}} + \omega \boldsymbol{g}$$

Because of the finite size, and the symmetry, of the system, the preferred direction $\boldsymbol{g}$ cannot be constant. A preferred circular direction is defined by a point c on a circle of radius 7 cm at depth 3 mm from the surface. The position c is updated continuously around the circle with a speed v_c that matches the average speed of the VF.

$$\boldsymbol{v}_c = \frac{V_0}{t_{tb} t_c}\left(1 - e^{-\frac{t_{tb}}{t_c}}\right) = 0.1\text{m} \times \text{s}^{-1}$$

For each RF, nine different values of omega for the VF were tested

$$\omega = 0,\ 0.2,\ 0.4,\ 0.6,\ 0.8,\ 1,\ 2,\ 4 \text{ and } 100$$

Every 10 min, a new value of omega was picked once, in random order, so that the same fish can experience the range of ω (social feedback). The direction of rotation clockwise (CW) or counterclockwise (CCW) was picked at random for each stimulus.

Drosophila *post experiments.* Multiple mixed male and female flies of 4 d of age were used for each experiment. 20–25 flies were introduced into the arena in the evening. Experiments ran from 18:00–10:30. Each condition was tested for 5 min and then changed sequentially. Experiments were performed at room temperature, 22–25 °C.

The physical post was 1 m high and 10 cm diameter and made from gray PVC pipe. The virtual post was generated using blender and styled to have the same color as the real post. In the virtual-post condition, the gray virtual post was placed inside a virtual cylinder with a checkerboard texture and with the same diameter as the FlyCave arena. This textured cylinder prevented the flies from flying into the walls. In real-post experiments, the real post was placed into the arena, and the gray virtual post was not shown. In the no-post condition, the checkerboard texture was replaced with a gray texture the same color as the post. In validation experiments with no added latency (**Fig. 2b**), the texture of the cylinder was controlled vertically (see following section) to elicit longer flight trials. In experiments to compare turning response of the flies in VR and RW, the texture of the cylinder was static.

Sample size was not predetermined. As each experiment contained multiple flies (20–30), we performed experiments until top views of the trajectories covered the arena densely.

Starting and stopping criteria. When one or many *Drosophila* were in flight, the experimental node chose the first one whose altitude met the geometric criteria $0.1\ \text{m} < z$ (altitude) < 0.9 m and whose distance from the center of the arena was < 0.35 m.

Trials were stopped when the active fly average speed over 5 s was less than 4 cm/s, when the active fly performing the trial had not been detected for 0.5 s, or when the stimulus condition changed.

Drosophila *path-following experiments.* Female flies of 4 d of age were used for each experiment. Experiments ran overnight, and multiple conditions were alternated as per *Drosophila* post trials.

To elicit the optomotor response, and thus path following, a stimulus was designed that placed the fly at the center of a virtual textured cylinder. The cylinder was textured with a black and white checkerboard texture to give a strong behavioral response. The origin of the cylinder was fixed at the position of the active fly so as to eliminate translational optical flow. The angular velocity, ϕ, of the textured cylinder surrounding the active fly was calculated by a closed-loop angular proportional control law[47] which tries to align the velocity vector of the fly with vector connecting the current fly position with a target point on the path. A second closed-loop attitude control law also biases the vertical motion of the cylinder to keep the flies at the same altitude in the arena. More exactly,

$$\phi = V_k * \theta_{\text{err}} * K$$

$$V_z = (0.8 - Z_{\text{fly}}) * K_{\text{vertical}}$$

Where V_k = max (1.0, V * 20) increases the gain for slowly flying flies. $\theta_{\text{err}} = \theta_{fly} - \arctan(|x_{\text{target}} - x_{fly}|, |y_{target} - y_{fly}|)$ is the angular error between the fly velocity vector and the current position minus the target position vector, K is the feedback gain for path following, and K_{vertical} is the feedback gain for altitude control. See **Supplementary Figure 7** for the influence of different gain values on path following behavior in *Drosophila*. When the active fly position was within 0.1 m of the target position, the target position was advanced to the next point along the path.

Sample size was not predetermined. Because the flight activity of the nonglued flies was higher than that of the head-fixed flies, we ran double the number of head-fixed fly experiments to increase number of trajectories analyzed.

Starting and stopping criteria. As per *Drosophila* trials.

Drosophila *tethered experiments.* Female flies of 4 d of age were used for each experiment. Flies were anesthetized by cooling to 3.2 °C on a custom-built thermoelectric cold plate (IMP Mechanical Workshop, Vienna) and fixed to a tungsten tether rod with a small drop of blue-light solidifying glue (Bondic). Depending on the preparation, the head was additionally bonded to the thorax. Flies were allowed at least 20 min recovery time before the experiments.

Rigidly tethered flies are placed in the center of a ping-pong ball used as a spherical projection screen for visual stimuli as described in ref. 48. Flies were filmed from above using a single camera. Estimation of right and left wing beat amplitudes happened at 100 Hz. The difference between the right and the left wing beat amplitudes was converted to a turning torque and forward force. Applying these forces to a virtual agent gave the tethered fly the ability to control its virtual position in a planar 2D space.

An identical virtual world as per freeflight experiments was used (a textured cylinder of the same dimensions as the FlyCave).

Sample size was not predetermined. After pilot experiments indicated that head-fixed and head-free flies both performed path following, experiments were performed until an N comparable with prior free-flight experiments was obtained.

Starting and stopping criteria. Once the tethered fly had started flying (beating its wings), trials were started by warping the virtual fly somewhere inside the virtual cylinder volume. Trials ended when the tethered subject stopped beating its wings or exited the virtual cylinder volume.

Mice. Experiments were performed in which mouse position was measured to determine locations avoided or preferred by mice (**Fig. 2**). The locations of shallow and deep relative to the experimental room were switched between trials, thus allowing us to check for effects from the checkerboards and the distal environment.

Experiments were performed at room temperature, 22–25 °C, from 11:30–18:00. Sample size was chosen based on effect strength of similar elevated plus-maze experiments. We elected to test 15 mice per condition or until our stock of suitable mice were exhausted.

Starting and stopping criteria. Mice were placed at the border between the shallow and deep sides and left for 15 min or until they jumped from the platform. Mice which jumped before 10 min were excluded from further analysis (N = 1 mouse jumped before completion of 10 min). Only naive mice were used. Mice were used for only one experiment.

Animal tracking. *Fish and fly tracking.* Multicamera tracking software called Flydra was used[18]. This software operates by updating a six-dimensional estimate (3D position and velocity) of animal state based on observations from each camera on every frame. The state update operation is done using an extended Kalman filter in which the motion model of the animal is a linear constant velocity model, and the nonlinear observation model is derived from the camera calibration and is linearized about the a priori predicted animal position on each frame. Camera calibrations are done using MultiCamSelfCal[49].

To track fish underwater in 3D with cameras out of water, we developed a new capability of correcting for refraction at the air–water interface. The nonlinear observation model described above was augmented with a model of the water surface and the refractive indices of water and air. Fermat's principle of least time and the camera calibration were used to calculate forward and reverse models of a 3D point underwater leading to a pixel on the image sensor.

Mouse tracking. Mouse tracking software is implemented using Python and OpenCV. Detection and tracking of head position is implemented using the following sequence of image processing operations operating at 120 fps (**Supplementary Video 11**).

(1) The incoming image is Gaussian blurred (sigma = 0.7)
(2) The foreground/background model (OpenCV MOG2, varThreshold = 0.8) is updated
(3) The largest contour from the foreground is extracted and simplified (cvApproxPolyDP, sigma = 1)
(4) The contour is filled and rotated into a landscape orientation
(5) The 'heavy' end of the contour is extracted (representing the head of the mouse)
(6) The extremity of the heavy end of the contour in the x-axis, and the mean (weighted center-of-mass) of the contour in the y-axis is taken to be the head of the mouse
(7) If the x- or y-position of the head has moved more than 30 pixels since the last frame, ignore the measurement
(8) Otherwise, use the mouse head position is used to update a Kalman Filter (constant motion model, process_noise = 3, measurement_noise = 300). Measurement update covariance (R) was chosen dynamically based on the elongation of the mouse contour—with head position estimates from elongated mice trusted more. If no head could be detected then the mouse head position is predicted based on the last position.

(9) The head x-, y-position in pixels is converted to the position in world coordinates by a scale factor. The head z-position is fixed at 0.14 m (the height of the platform).

Data preparation and data handling. *Lagged correlation measure.* The Pearson correlation was used to measure the relationship between visual system input and behavioral output. The correlation was computed at different time lags (by shifting the system output with respect to the system input) in order to account for the closed loop latency the system, and to characterize how the organism response to stimulus changes over time. Lagged Pearson correlation was used rather than cross-correlation to deal with time series of different lengths and with missing data.

Zebrafish. Trials shorter than 1 s were discarded. In path-following experiments, all remaining data were then split into 1 s segments for further analysis. Lagged correlations were computed for each 1 s segment; these lagged correlations were then averaged to give one lagged-correlation series per fish and again one per condition.

In post experiment trials associated with **Figure 1**, observations where the 3D position estimate had been obtained from only one camera were removed.

For comparisons of lagged correlations between groups, variances were checked to not differ. Under large dots, where no difference between genotypes was found: Mann–Whitney test $P = 0.52$, Bartlett's test of equality of variance $P = 0.42$. For small dots, where a difference between genotypes was observed: $P = 0.014$, equality of variance $P = 0.15$. For gray condition where no difference between genotypes was observed: $P = 0.82$, equality of variance $P = 3 \times 10^{-8}$; however, the equality of variance P value is on account of no overall responses.

Drosophila post trials. For all experimental groups, trials shorter than 2 s were discarded. Trials were truncated when z-position was outside the range $0.1 \text{ m} < z < 0.9$ m (flies sitting on the floor or ceiling of the arena). Trials were truncated when the lateral (x,y) distance from the center of the cylinder to the fly exceeded 0.42 m (flies sitting on the walls of the cylinder). Trials were truncated when the fly forward velocity was ≤0.05 m/s (experimentally determined to represent when flies landed on the post or walls). In trials associated with **Figure 1**, observations where the 3D position estimate had been obtained from only one camera were removed.

Drosophila *path-following trials.* For all experimental groups, trials shorter than 1 s were discarded. Trials were truncated when z-position was outside the range $0.1 \text{ m} < z < 0.9$ m (flies sitting on the floor or ceiling of the arena). Trials were truncated when the lateral (x,y) distance from the center of the cylinder to the fly exceeded 0.42 m (flies sitting on the walls of the cylinder). Trials were discarded when >50% of the trial had a mean forward velocity of ≤0.05 m/s (experimentally determined to represent walking trajectories). Observations where the 3D position estimate had been obtained from only one camera were removed.

46. Bastien, R. *et al.* KymoRod: a method for automated kinematic analysis of rod-shaped plant organs. *Plant J.* **88**, 468–475 (2016).
47. D'Azzo, J.J. *Linear Control System Analysis and Design: Conventional and Modern* (McGraw-Hill, 1995).
48. Fenk, L.M., Poehlmann, A. & Straw, A.D. Asymmetric processing of visual motion for simultaneous object and background responses. *Curr. Biol.* **24**, 2913–2919 (2014).
49. Svoboda, T., Martinec, D. & Pajdla, T. A convenient multicamera self-calibration for virtual environments. *PRESENCE Teleoperators Virtual Environ.* **14**, 407–422 (2005).